MEC-Assisted Panoramic VR Video Streaming Over Millimeter Wave Mobile Networks

Yanwei Liu, *Member, IEEE*, Jinxia Liu, Antonios Argyriou, *Senior Member, IEEE*, and Song Ci, *Senior Member, IEEE*

***Abstract*—Panoramic virtual reality video (PVRV) is becoming increasingly popular since it offers a true immersive experience. However, the ultra-high resolution of PVRV requires significant bandwidth and ultra-low latency for PVRV streaming, something that makes challenging the extension of this application to mobile networks. Besides bandwidth, the frequent perspective viewport rendering induces a heavy computational load on battery-constrained mobile devices. To attack these problems jointly, this paper proposes a PVRV streaming system that is designed for modern multiconnectivity-based millimeter wave (mmWave) cellular networks in conjunction with mobile edge computing (MEC). First, mmWave is deployed to support the high bandwidth needs of PVRV streaming. Next, the multiple mmWave links that tend to suffer from outages are coupled with a sub-6 GHz link to ensure disruption-free wireless communication. With the help of an MEC server, the tradeoff among link adaptation, transcoding-based chunk quality adaptation, and viewport rendering offloading is sought to improve the wireless bandwidth utilization and mobile device's energy efficiency. Simulation results show that the proposed scheme can improve the streaming performance in both energy efficiency and the quality of received viewport over the state-of-the-art schemes.**

***Index Terms*—Link adaptation, millimeter wave mobile networks, mobile edge transcoding, panoramic VR video, viewport rendering offloading.**

I. Introduction

IN RECENT years, the convergence of advanced virtual reality (VR) technologies and fast video processing hardware has created a totally new media form, namely the immersive panoramic (360-degree) VR video. Panoramic VR video (PVRV) can provide a 360-degree view angle to obtain an omni-directional viewport of the scene and consequently it is particularly suitable for events like exhibitions, sports, concerts and films [1].

A key feature of PVRV is the ultra-high spatial resolution. This means that an extremely unprecedented amount of data is generated and must be delivered to a user. However, this has not been a problem until now since even though PVRV applications are rapidly increasing, most of the PVRVs are watched offline (video is completely downloaded and viewed locally by moving the viewport in real-time). At the same time mobile displays are becoming better by the day and an increasing number of people prefer to experience PVRV at any time and any place [2]. Hence, similar to other types of video, PVRV will have to be delivered over a network. In addition, users today consume their media through wireless mobile devices. Consequently, the combination of a very high data rate demand by PVRV with a bandwidth-limited and error-prone wireless channel is a recipe for poor quality-of-experience (QoE) in PVRV delivery.

By looking at the problem of wireless PVRV streaming we notice that it can be broken down to three fundamental challenges. The first challenge is that the available bandwidth for PVRV delivery over wireless networks is a limited resource due to multi-user channel access. Ultra-high resolution PVRV typically requires a bandwidth that is $4\sim 5\times$ of what is used for delivering a regular high-definition (HD) video [3]. Even current state-of-the-art video coding standards like H.265/HEVC can improve compression efficiency relative to the past, but the data rate of PVRV after compression is still very high for current wireless networks. For example, the data rate of PVRV for an advanced experience is typically more than 350 Mbps. Hence, when multiple PVRV applications compete for one network, the data rate requirement for the network will be up to several Gbps [4]. Even for a basic experience, the data rate of PVRV for a single user can reach up to 20 Mbps [4]. To cater for the high bandwidth demand of such *elephant* flows, next generation wireless networks (5G) focus on using spectrum resources that were unused in previous communication standards.

The second major challenge is that PVRV applications must perform a pixel-by-pixel computation of the viewport rendering [5] on the mobile device or the head mounted display (HMD). Fig. 1 illustrates in detail the process of viewport rendering. A certain region of data in PVRV is extracted (pixel position A), then transformed into a spherical port (pixel position B), and finally projected to the viewport plane (pixel position C). This operation requires pixel-by-pixel position transform with ma-

Manuscript received March 2, 2018; revised June 28, 2018 and August 14, 2018; accepted September 22, 2018. Date of publication October 15, 2018; date of current version April 23, 2019. This work was supported in part by the National Natural Science Foundation of China under Grant 61771469 and Zhejiang Provincial Natural Science Foundation of China under Grant LY17F010001. The associate editor coordinating the review of this manuscript and approving it for publication was Dr. Shiwen Mao. (*Corresponding author: Jinxia Liu.*)

Y. Liu is with the State Key Lab of Information Security, Institute of Information Engineering, Chinese Academy of Sciences, Beijing 100049, China, and also with the School of Cyber Security,University of Chinese Academy of Sciences, Beijing 100049, China (e-mail: liuyanwei@iie.ac.cn).

J. Liu is with the Zhejiang Wanli University, Ningbo 315100, China (e-mail: liujinxia@zjwu.edu.cn).

A. Argyriou is with the Department of Electrical and Computer Engineering, University of Thessaly, Volos 382 21, Greece (e-mail: anargyr@uth.gr).

S. Ci is with the University of Nebraska-Lincoln, Omaha, NE 68046 USA (e-mail: sci@engr.unl.edu).

Color versions of one or more of the figures in this paper are available online at http://ieeexplore.ieee.org.

Digital Object Identifier 10.1109/TMM.2018.2876044

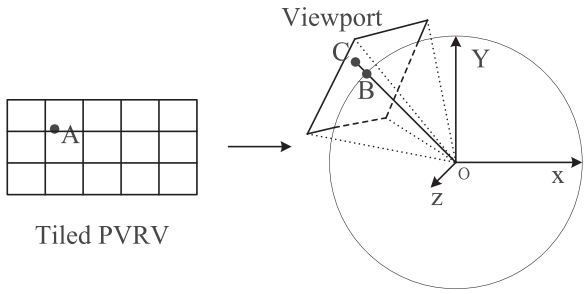

Fig. 1. Illustration of viewport rendering.

trix computations. Since these types of devices are powered by batteries, this type of computation consumes power from the mobile device that is unlike any other form of video playback. Unfortunately battery capacity is always a limited resource in mobile devices and so it is impossible to render a PVRV for an extended time period.

A third problem is that intermediate processing for PVRV playback increases latency, something that is considerably different from the classic video streaming applications. To be more precise, when PVRV is requested interactively by the end-user, several intermediate communication and computing processing operations are needed to provide the user with the requested viewport, i.e., PVRV transmission over the network (from source provider to user equipment), PVRV decoding, and frequent viewport rendering on user equipment (UE) that are caused by dynamic viewport changes. These operations are finished with a significant computational cost that generates an additional end-to-end latency. Generally, the transmission of PVRV in full resolution can significantly contribute to the end-to-end latency. Current immediate PVRV computing operations can take as much as 6$\sim$100 ms, and communication delay (source provider to user equipment) can reach 10$\sim$200 ms. Since HMD updates the viewport data very quickly, typically with a frequency between 60 Hz and 120 Hz [6], HMD requires an strict latency bound about 20 ms for data input. Thus, the increase of the end-to-end latency will degrade the QoE of interactive PVRV playback significantly.

To deal with the above challenges, past research efforts were on PVRV streaming schemes by looking at the problem both from a compression and a networking perspective. However, most of the approaches in the past aimed at wireline transmission or offline viewing and they were not concerned with wireless access which is a key part of modern networks.

At the same time that video communication technology is moving forward with PVRV, wireless communication pushes into the future with millimeter Wave (mmWave) systems. In 5G systems mmWave provides ultra-low latency and high bandwidth [7]. However, the mmWave channel is prone to outages since it requires line-of-sight (LOS), i.e., different physical obstacles in the environment may break completely the link. To make up for the uncertainty of mmWave communication, existing sub-6 GHz frequencies band can be used as a backup for the mmWave band. A fast handover architecture among mmWave and sub-6 GHz links has already been successfully tested for UDP applications [8]. This dual radio architecture is envisioned to be typical in 5G systems. Naturally, mmWave can be used to transmit high bitrate PVRV to meet the ultra-low delay requirement for viewport requests. However, PVRV requires interactive playback of viewport. This characteristic of PVRV emphasizes the importance of a user-specific viewport region. In light of these advances a problem can be easily described: *how to adapt the unequally important regions in PVRV to the unsteady mmWave network for improving the streaming performance and user experience.*

While mmWave communication is the future of wireless access, the core wireline network is transformed by the mobile-edge computing (MEC) paradigm that is emerging as an efficient solution for content caching and in-network computing at the edge of mobile network [9]. In our case it offers a platform where we can investigate wireless PVRV streaming: First, MEC can be deployed near the macro or micro base-station (BS) as a cache server to push the PVRV data close to the mobile user. Thus, the video transmission delay can be reduced significantly. Second, MEC can reduce the computational load on the mobile device by providing computational resources to the UE. *In this paper we propose the tight coupling of MEC with the multi-connectivity (MC-based) mmWave cellular network so as to enable and optimize wireless PVRV streaming.* The contributions of the paper address one-by-one the previously mentioned challenges and are described next.

First, we propose the use of an MC-based mmWave/sub-6 GHz communication architecture as a basis for satisfying the high bandwidth demand of PVRV streaming. By fully exploiting the advantage of mmWave in terms of communication capacity, the sub-6 GHz frequencies band is used to compensate for the problems of rapid channel disruptions in the mmWave band. The proposed architecture is accompanied by algorithms for importance-based mmWave link adaptation with unequal-error protection and goodput-oriented sub-6 GHz link adaptation. Their joint operation ensures that the PVRV representation adapts smoothly to the fluctuating wireless conditions.

The second contribution is that MEC functionality is designed jointly with the PVRV streaming system so as to reduce system latency and the UE's energy consumption that are incurred by the viewport data decoding and rendering. More specifically we propose the use of an MEC server for proactive PVRV content caching, real-time PVRV transcoding, and finally low-latency and energy-efficient offloading of the viewport rendering. A key feature is that our MEC-based real-time PVRV transcoding considers region-based unequal bitrate allocation of the locally cached data. This transcoding offers the mmWave link uncompressed PVRV data that leads to reduction of the intermediate processing latency. Energy efficiency is accomplished because viewport rendering is selectively offloaded to the MEC server to reduce the energy consumption of the UE that is raised by the pixel-by-pixel viewport rendering. To the best of our knowledge, no previous research work has focused on improving energy-efficiency of mobile devices, together with lowering the latency of PVRV streaming.

Our third contribution is that we formulate a novel communication and computation resource allocation problem for the MEC server and the UE. The problem is shown to be a

multi-objective combinational optimization problem, subject to the viewing-delay constraint. More specifically, the transcoding chunk quality, the modulation and channel coding schemes (MCS) for different links, and the viewport rendering offloading determination parameter are calculated to maximize the viewport quality, while minimizing the energy consumption of the UE.

The rest of the paper is organized as follows. Section II provides a detailed analysis of the related work. In Section III, the system model of the proposed MEC-assisted PVRV streaming scheme over MC-based mmWave network is presented. The problem formulation and our solution approach are described in Section IV. Section V presents the simulation results. Finally, Section VI concludes the paper.

II. Related Work

A. PVRV Delivery

The spatial resolution of PVRV is considerably larger than HD video. Consequently, the delivery of high-quality PVRV to the mobile device is very challenging due to the bandwidth-constrained network. To save bandwidth, one could use high-efficiency compression techniques, e.g., H.264/AVC-based PVRV coding [10], and H.265/HEVC-based PVRV coding [11]. Since compression is closely related to data representation, the studies in [12] and [13] have proposed content-adaptive or viewport-centric-adaptive representations that offer flexible delivery options. To facilitate interactive viewport streaming, a tile-based/strip-based encoding scheme was proposed in [14]. For interactive PVRV streaming, only tiles within the field of view (FOV) are delivered to the end-user. Considering dynamic FOV, a viewport-dependent adaptive streaming system was proposed in [15] to reduce the bandwidth requirements. By exploiting the advantages of HTTP-based adaptive streaming, tiling-based PVRV streaming over DASH was also proposed to optimize QoE [16]–[18].

The previous studies are aimed primarily at wireline PVRV transmission or offline delivery with local viewing on the device. Current PVRV delivery mechanisms lack an optimized delivery that is tailored to wireless networks. Since mobile network capacity is gradually growing, it can accommodate multi-user PVRV traffic and lead to a new era of video communication. However, traditional mobile streaming schemes are not very efficient for PVRV due to the high bitrate of PVRV. Consequently, more sophisticated PVRV streaming schemes have to be designed for emerging mobile wireless networks.

B. Video Communication Over mmWave

Recent advances in mmWave wireless communication allow for the support of high throughput applications. Preliminary results indicate that a high data-rate mmWave link can communicate ultra-low delay and uncompressed video traffic without problems [19]. However, one of the key challenges of mmWave communication is channel dynamics: The channel varies rapidly and the link maybe completely broken due to non-LOS paths between the transmitter and the receiver. For video traffic over mmWave, the authors in [20] proposed to use a receiver buffer and data transmission scheduling for video bitrate adaption that matches the channel. In another work [8], an MC-based LTE-5G integrated architecture was proposed to improve the reliability of mmWave communication but not for video traffic. Classic techniques for low-delay video streaming with unequal error protection were proposed in [21] but in this case for a 60 GHz mmWave link. Similarly, by adopting network coding to enhance the packet transmission reliability, the work in [45] confirmed the feasibility of streaming video over cellular MC-based mmWave links.

Furthermore, two recent works have proposed the delivery of virtual reality game videos over mmWave networks. To cope with the problem of PVRV signal intermittence caused by blockages, the authors in [22] proposed to add a mmWave mirror device to relay the blocked signal, but they ignored the signal blockage problem of the added mirror device. In [23], the energy efficiency of a mmWave BS was optimized with dynamic power allocation for PVRV transmission.

The previously mentioned techniques exploit to the fullest mmWave communication for ordinary video traffic. However, they are not directly applicable to PVRV streaming since PVRV traffic has certain specific characteristics. Though the recent works have tried to optimize PVRV applications over mmWave networks, they were still focused on the mmWave network optimization and were not concerned with the particular characteristics of PVRV traffic. It is still unclear how PVRV streaming performance is related to the dynamics of an MC-based mmWave channel, when it is affected by image tiling and viewport changing.

C. Mobile Edge Computing

Modern mobile applications are sophisticated and usually have a high computational load. This is unacceptable for a power-limited mobile device. The rise of MEC makes up for the inability of mobile devices to dedicate computing resources for a protracted time period [24]. Mobile computation on the UE can be partially transferred/offloaded to the MEC server. Even though there have been studies on computational offloading in mobile networks, they did not focus on the internals of the communication system during computational offloading. Within the communication subsystem, link adaptation and video chunk quality selection can be jointly optimized with a trade-off between communication and computational offloading to further improve the system performance. Additionally, when the MEC architecture is extended to PVRV streaming, the system optimization problem needs to consider adaptive viewport rendering offloading.

III. System Model

The proposed PVRV streaming system consists of three key elements: the content provider, the MEC server and the MC-based mmWave/sub-6 GHz cellular network. We provide a brief overview of the overall system functionality in the first subsection. In the remaining subsections we discuss the necessary mathematical models for transcoding, the wireless links, and

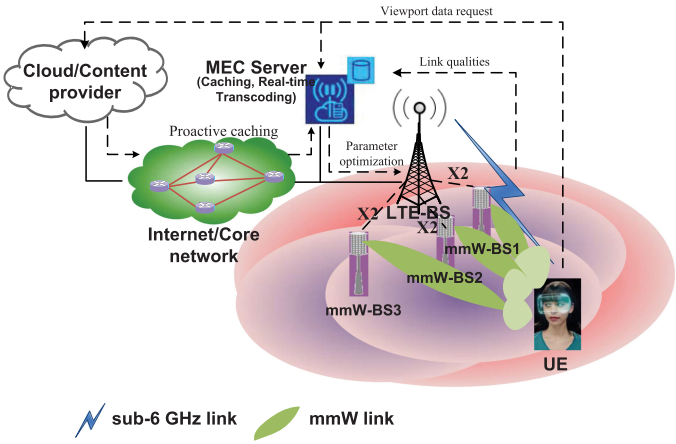

Fig. 2. MEC-assisted PVRV streaming system over the MC-based mmWave mobile networks.

their impact on latency and energy. Then, the resulting models are used in our optimization described in the next section.

A. System Overview

The content provider is responsible for storing the PVRV source content that is compressed. In the distribution network, caching for frequently requested content is enabled at the MEC server [26] which is located at the edge of the radio access network (RAN). When users within the coverage of the RAN request interactively the viewport data from the content provider, the requested data will be retrieved from the cache of the MEC server. In this work we assume that all PVRVs that the users request are available at the MEC server before performing the proposed optimization, and only one bitrate representation of a PVRV with the same quality for all tiles is cached at the MEC server.

The PVRV that is at the MEC server is delivered through the RAN that uses MC-based sub-6 GHz and mmWave links. The end-user uses a UE that is a multi-radio device that can simultaneously connect to the sub-6 GHz and mmWave links. This architecture is illustrated in Fig. 2, where the MEC platform is deployed near the sub-6 GHz BS in the RAN and acts as an intermediate server. At the MEC server, a PVRV transcoding module is in charge of the PVRV transrating for adapting to the sub-6 GHz link dynamics and also provides the uncompressed PVRV for the mmWave link. During the interactive request of PVRV, the user's viewport changes rapidly. To avoid a large motion-to-photon latency in the HMD, the full-resolution video is fetched at the HMD.

Regarding the cellular network, both the mmWave and sub-6 GHz bands are enabled. As shown in Fig. 2, the sub-6 GHz BS is used as a master BS and the mmWave BSs is the secondary BSs. The mmWave BS can communicate with the sub-6 GHz BS through an X2 link. The transmitted data packets over the sub-6 GHz and mmWave links converge at the integrated packet data control protocol (PDCP) layer in the user plane. The mmWave link with the maximal signal interference to noise ratio (SINR) is selected among all the available that are not in outage. Alternatively, when none of the available mmWave links can satisfy the transmission requirements, the sub-6 GHz link is used as a backup.

In this work we also exploit the radio network information service (RNIS) that is available for authorized mobile edge applications. RNIS can collect not only the radio network information but also the context information regarding UEs connected to the radio nodes that associated with the mobile edge host [25]. In our system with the help of RNIS, the MEC server estimates periodically the wireless sub-6 GHz link quality, and collects the device power information and the viewport information for a given UE. On the other hand the mmWave downlink quality is estimated from the uplink sounding reference signals that are periodically broadcasted from the UE over the whole angular space.

Based on the collected link quality information and user's viewport information, the MEC server first performs link selection and then executes link adaptation and viewport rendering offloading optimization for the selected link. In the optimization, the PVRV quality, wireless link adaptation and computational resources on the MEC server are jointly selected under the given latency limitation. For wireless link adaptation, a goodput-oriented MCS selection for the sub-6 GHz link and an importance-based MCS selection for the mmWave link are performed to optimize the overall wireless transmission performance.

After that, the information of the selected link and the optimization result will be sent to the UE. The UE will make the specific request to the appropriate BS for the correct chunk quality depending on the optimization result. Finally, the MEC server will configure the actual communication and computation subsystems to satisfy the user's request.

B. Mobile Edge Transcoding

To provide the appropriate data representations for different links, a real-time transcoding module is designed, as shown in Fig. 3. Originally, PVRV is encoded with spatial tile partitioning to facilitate viewport cropping. The stream of each tile is then segmented into chunks temporally. During transcoding, a chunk from the original PVRV stream is first decoded into uncompressed video that includes the viewport-covered tiles and the non-viewport tiles. Based on the periodic feedback of the available channel goodput, the appropriate quantization parameters (QPs) are selected in terms of the rate-quantization relationship [27], and then used to re-encode the viewport tiles and non-viewport tiles. Uncompressed PVRV data including viewport data are transmitted over the high-speed mmWave link, while compressed PVRV data including the viewport data are transmitted over the sub-6 GHz link when all the mmWave links are in outage.

After transcoding, two candidate PVRV representations are available to be transmitted over the sub-6 GHz link, as shown in (A) and (B) in Fig. 3. For the full-resolution video to be delivered over the sub-6 GHz link, the tiles within the viewport region may be transcoded into a higher-quality viewport stream on the MEC server. The remaining tiles outside the

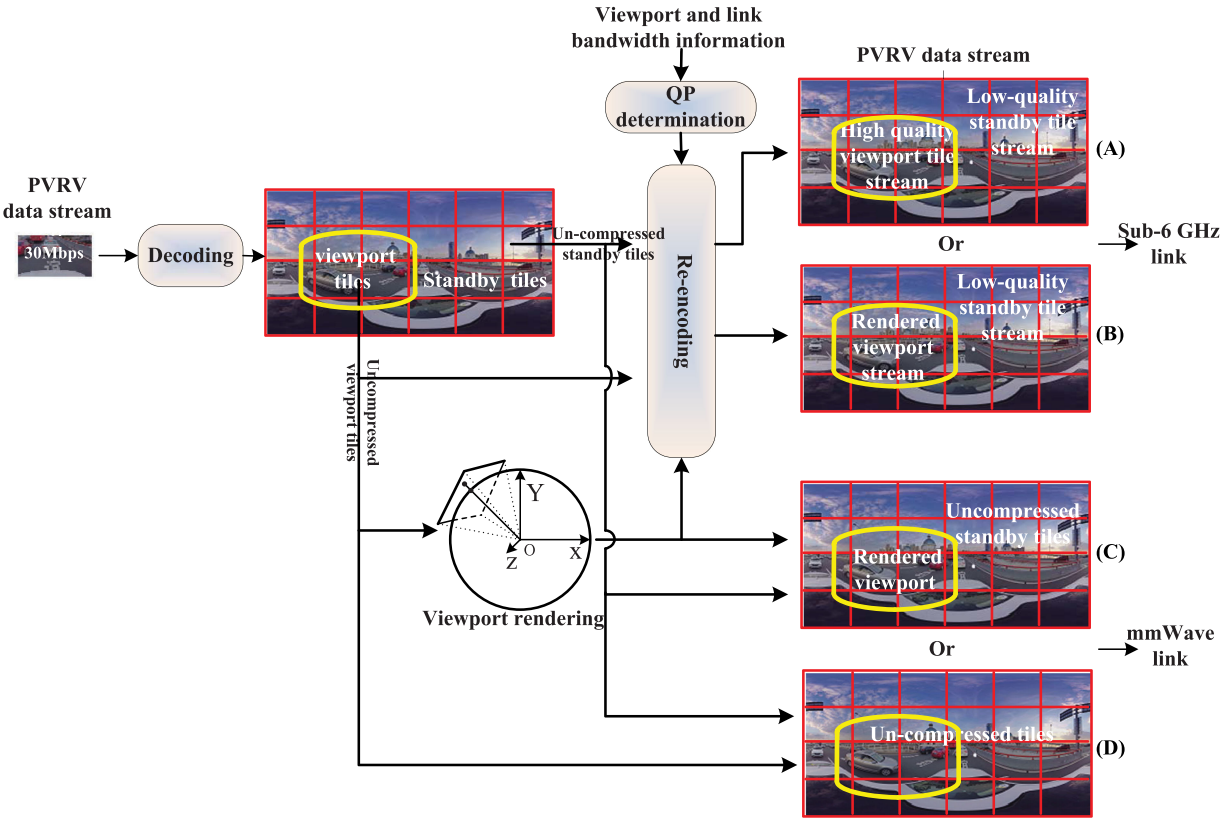

Fig. 3. The proposed MC-based mobile edge transcoding framework supports different wireless transmission links.

viewport will be allocated with a lower quality and will be used as standby tiles. When the viewport data cannot keep pace with the fast viewport changes, the standby tiles with a lower quality are projected to the necessary viewport at the mobile device for smoothing viewport transition. Thus, the data of the rendered higher-quality viewport, together with the remaining lower-quality standby tiles constitute the full-resolution video ((B) in Fig. 3) that will be delivered to the UE. Besides viewport rendering on the MEC server, another candidate PVRV representation renders the viewport locally on the mobile device. In this case, the tiles within the viewport are compressed in an appropriate quality and together with the compressed standby tile data ((A) in Fig. 3) are delivered to the UE. The output data stream from the transcoder is segmented into a series of chunks with a duration of one group of pictures (GOP) that consists of four frames. This relatively short chunk allows us to trade-off PVRV compression performance and data synchronization efficiency at the HMD.

Regarding the viewport quality it is controlled by the transcoding bitrate that depends on the selected QP. To formally capture the above, we use q_o to denote the quality of the original bitrate representation of PVRV that is already cached at the MEC server, and the vector $\pi_i^{trs}, i = 1, \ldots, N^{trs}$ denotes the set of transcoded bitrate representations of PVRV, where N^{trs} is the number of the transcoded bitrate representations. The quality set for the tiled chunks after transcoding is denoted as $Q^{trs} = q_i(\pi_i^{trs}), i = 1, \ldots, N^{trs}$, where $q_1(\pi_1^{trs})$ is the highest quality and $q_{N^{trs}}(\pi_{N^{trs}}^{trs})$ is the lowest quality.

For the mmWave link, there are also two candidate data representations for transmission, as shown in (C) and (D) in Fig. 3. One is the uncompressed full-resolution PVRV ((D) in Fig. 3). In this case viewport rendering will be performed locally at the mobile device. Another data representation is a rendered viewport plus the uncompressed standby tiles ((C) in Fig. 3). For this representation, the viewport is rendered on the MEC server. Obviously, the quality of the viewport and the quality of the uncompressed standby tiles are both determined by quality q_o.

C. Communication Model

The sub-6 GHz and mmWave link work in a time-division multiplexing mode. Next we describe their operation in detail.

1) MC-based mmWave Communication: For the mmWave link, its quality is tracked in real-time to calculate the probability of link intermittence. By predicting the availability of each mmWave link, we schedule the time slots to different links through a coordinator that is located at the sub-6 GHz BS. The metric used for selecting the mmWave link is the instantaneous SINR from the BS to the UE. Each UE broadcasts directionally uplink sounding reference signals to the mmWave BS. The uplink sounding reference signal is then used to estimate the mmWave downlink channel quality. The mmWave BS also needs to align its beam direction with the UE to find the best transmission direction. The corresponding SINR for the best alignment is recorded and sent to the coordinator. The coordinator reports the optimal transmission direction and the SINR

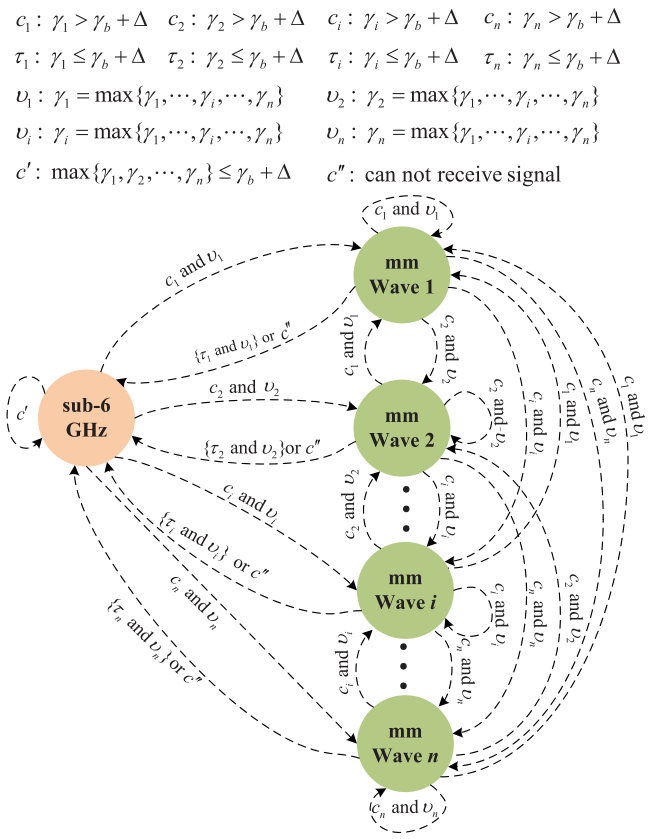

Fig. 4. Scheduling of MC-based mmWave and sub-6 GHz links. Green circles indicate the mmWave band communication states and pink circle indicates the sub-6 GHz band communication state. The arrows indicate the transitions from one communication state to another state when the corresponding transition condition is satisfied.

value of the mmWave link to the UE via the sub-6 GHz link. If all the mmWave BSs cannot receive synch or reference signals from the UE or the SINR values of all the mmWave links cannot meet the desired transmission requirement, the sub-6 GHz link will be used to transmit the application data.

To model the previous communication system, we denote with γ_b the LOS (line-of-sight) baseline SINR value. If the SINR value of the mmWave link is less than $\gamma_b + \Delta$, then mmWave is considered to be in the NLOS (non-line-of-sight) state (that the mmWave link may be blocked). Δ is a scaling factor that accounts for the SINR decrease in the blocking state compared to the un-blocked state [8]. Also $\gamma_1, \gamma_2, \ldots, \gamma_n$ indicate the SINR values of the $1, 2, \ldots, n$ mmWave links. Link switching is illustrated in Fig. 4. In Fig. 4, we assume that n mmWave bands and one sub-6 GHz band are available for communication, and $c_1, \ldots, c_n, \upsilon_1, \ldots, \upsilon_n, \tau_1, \ldots, \tau_n, c'$ and c'' are a series of transition conditions for different communication states. When the transition conditions are satisfied, the communication link will be switched to the next mmWave communication link.

2) Goodput-oriented sub-6 GHz Link Adaptation: The expected effective goodput for a wireless link is defined as the ratio of the expected delivered data payload to the transmission time. Clearly, depending on the data payload length and the wireless channel conditions, the expected effective goodput varies with different transmission strategies. The more robust the transmission strategy, the more likely the data will be delivered successfully with fewer retransmissions. The key idea of goodput-oriented link adaptation is to select the most suitable transmission strategy for the current channel conditions.

In this work, Release 12 of Long Term Evolution-Advanced (LTE-A) [28] is considered as the sub-6 GHz communication system. In the LTE downlink, the available goodput for transmitting video chunks depends primarily on the link quality, the selected MCS mode and the number of the allocated resource blocks (RB). Typically, the number of available RBs is estimated based on the ratio of user's minimum data rate requirement to the channel gain [29]. Consequently, the achieved goodput for a given user depends on the link quality and the selected MCS mode once the number of RBs is determined. To estimate the goodput $G_{sub-6GHz}(m)$ for the sub-6 GHz link, the mutual information effective SINR mapping $\Psi(m)$ is utilized to measure the downlink quality as [30]

$$\Psi(m) = \upsilon(m) \left[\Upsilon^{-1} \left(\frac{1}{S} \sum_{i=1}^{S} \Upsilon \left(\sqrt{\frac{\varphi_i}{\upsilon(m)}} \right) \right) \right]^2, \quad (1)$$

where S is the number of allocated subcarriers, φ_i is the SINR value at the ith subcarrier, and $\upsilon(m)$ is the calibration factor for MCS mode m. The mutual information functions $\Upsilon(\cdot)$ and $\Upsilon^{-1}(\cdot)$ are defined as (9) and (10) in [30]. Based on $\Psi(m)$, the Block Error Rate (BLER) $\theta(\Psi(m))$ is estimated as

$$\theta(\Psi(m)) = \frac{1}{2} erfc \left(\frac{\Psi(m) - b(m)}{\sqrt{2} c(m)} \right), \quad (2)$$

where $erfc(\cdot)$ is the complementary error function, $b(m)$ and $c(m)$ are the "transition center" and "transition width", respectively.

Due to the truncated automatic repeat request (ARQ) mechanism, RBs that are received in error during the original transmission might be retransmitted up to a maximum of N_r times. In the LTE system, Chase Combining (CC) and Incremental Redundancy (IR) can be used for data retransmission. In this work, we assume that chase combining with reduced half size retransmission is used [31] and each retransmission uses the same MCS mode with the original transmission, thus $\varepsilon(m) = \theta(\Psi(m))$ and the average number of transmissions per RB can be calculated as:

$$\bar{N}(\varepsilon(m), N_r) = \sum_{i=1}^{N_r} i \cdot (1 - \varepsilon_i(m)) \cdot \prod_{j=0}^{i-1} (\varepsilon_j(m)) + 1 \quad (3)$$

The information bits contained in each symbol is $r(m) = R_c \cdot \log_2(H_m)$, where R_c is the forward error correction code rate and H_m refers to a H_m-QAM constellation for MCS mode m. Usually, each RB contains 7 OFDM symbols in the time domain and 12 subcarriers in the frequency domain. Therefore, the information bits carried per RB for an MCS mode m is $\ell(m, N_r) = 12 \cdot 7 \cdot r(m)$. When truncated ARQ is adopted, each RB is transmitted $\bar{N}(\varepsilon(m), N_r)$ times on average. Assuming that the total number of RBs B_{num} is allocated for delivering one video chunk and that all the RBs adopt the same MCS mode,

the achieved goodput of the sub-6 GHz link is

$$G_{sub\text{-}6GHz}(m) = \frac{\sum_{i=1}^{N_r}\left[\frac{1}{2^i}\cdot \ell(m,N_r)\cdot B_{num}\cdot(1-\varepsilon_i(m))\cdot\prod_{j=0}^{i-1}(\varepsilon_j(m))\right]}{\bar{N}(\varepsilon(m),N_r)} + \frac{\ell(m,N_r)\cdot B_{num}}{\bar{N}(\varepsilon(m),N_r)} \quad (4)$$

3) Importance-based mmWave Link Adaptation: For uncompressed PVRV the tiles have different importance levels to satisfy the demand of transient viewport viewing [32]. The tiles within the viewport at the precise time instant of PVRV viewing are more important than the remaining tiles outside the viewport. With bit-interleaving, the RGB data of the uncompressed PVRV are further grouped into the most significant bits (MSBs) and least significant bits (LSBs) for transmission.

At the physical layer of the mmWave link the MCS can be configured to provide different error-resilience and transmission capacities. Hence, we propose an importance-based MCS adaptation scheme by considering the different importance levels of the bit data in different tiles of the image. Note that a mmWave link in 5G adopts different protocol design from an LTE-A system. To capture the characteristics of the mmWave link more accurately we adopt a different link abstraction from the sub-6 GHz link. In one mmWave transmission slot, the transmission block (TB) is composed of several coding blocks. Thus the error rate of the coding blocks directly affects the quality of the received video. Based on the mean mutual information per coded bit (MMIB), the BLER for each codeblock (CB) can be modeled with a Gaussian cumulative model similarly to (2),

$$C_{BLER,\,i}(x_i) = \frac{1}{2}erfc\left(\frac{x_i - b_{Csize,m}}{\sqrt{2}c_{Csize,m}}\right), \quad (5)$$

where $C_{BLER,\,i}(x_i)$ is the BLER at x_i and x_i is the MMIB for the ith CB with MCS mode m in one TB. Parameters $b_{Csize,m}$ and $c_{Csize,m}$ are the mean and standard deviation of the Gaussian distribution [33], [44]. Then, the BLER for one TB that contains I CBs is

$$T_{BLER} = 1 - \prod_{i=1}^{I}(1 - C_{BLER,i}(x_i)). \quad (6)$$

To control the BLER of different tiles of the image, the appropriate MCS is selected for each TB in term of its level of importance. Assume that the MCS are ranked in an ascending order. Hence, larger MCS can provide higher transmission rate with lower protection strength and fewer redundancy bits. In the proposed scheme, according to the viewport requesting information, the viewport tiles and non-viewport tiles are first identified on the MEC server. As shown in Fig. 5, bit-interleaving will generate different TBs with four importance levels. We sort these levels in a decreasing order as: MSBs of the viewport tiles (MSBV), LSBs of the viewport tiles (LSBV), MSBs of the standby tiles (MSBS), and LSBs of the standby tiles (LSBS). The sequentially decreasing MCSs are selected accordingly for the TBs. Assume that MCS m_{mv} is selected for a TB that belongs to a MSBV and $m_{\max}$ denotes the maximal MCS index

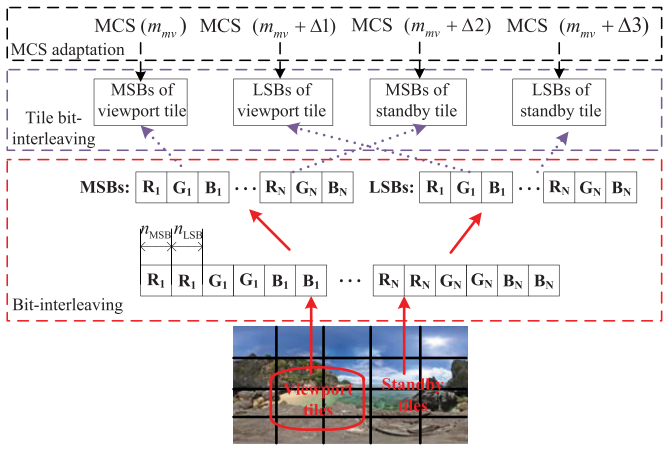

Fig. 5. The importance-based link adaptation. The red solid line arrow indicates the bit-interleaving processing, the purple dot line arrow indicates the tile bit-interleaving processing and the black dash line arrow indicates the importance-based MCS adaptation.

in the candidate MCS set. The intervals between m_{mv} and the MCSs of LSBV, MSBS, and LSBS are $\Delta1$, $\Delta2$, and $\Delta3$, respectively. In this paper, after performing extensive tests in a 5G mmWave simulation module [33], [44], we empirically set $\Delta1 = 1$, $\Delta2 = 3$, and $\Delta3 = 5$. Thus, the MCS m for one TB is selected as

$$m = \begin{cases} m_{mv}, & \text{if the TB belongs to MSBV} \\ \min(m_{\max}, m_{mv}+\Delta1), & \text{if the TB belongs to LSBV} \\ \min(m_{\max}, m_{mv}+\Delta2), & \text{if the TB belongs to MSBS} \\ \min(m_{\max}, m_{mv}+\Delta3), & \text{if the TB belongs to LSBS} \end{cases} \quad (7)$$

The size T_{size} of one TB with an associated MCS m can be obtained based on the total number of subcarriers per RB (derived from the customized configuration of each user), the number of symbols per slot, and the number of reference symbols per slot [33], [44]. In a practical environment, the mmWave MIMO channel may suffer from poor spatial diversity that results in lower capacity due to the deficiency of parallel information paths. The recent work in [46] confirmed that with molecular absorption, the MIMO capacity increases linearly as the number of antennas increases. Consequently, when no retransmission scheme is used (for low-latency), the transmission goodput $G_{mmW}(m)$ for one TB over a $K \times K$ MIMO mmWave channel is calculated as

$$G_{mmW}(m) = (1 - T_{BLER})\cdot 1000 \cdot T_{size}\cdot(\lambda_f \cdot K + b_f), \quad (8)$$

where λ_f and b_f are two parameters for fitting the linear relationship between the MIMO capacity and the number of antennas K at mmWave frequency f. In this paper, we adopt $\lambda_f = 0.184$ and $b_f = 0.816$ (In terms of [46, Fig. 7]) for a 73 GHz mmWave MIMO channel.

D. Latency and Energy Model

The perspective viewport can be rendered on the MEC server or locally on the mobile device. These approaches will result in different energy consumption and transmission latency that must

TABLE I
NOTATIONS IN SUBSECTION D OF SECTION III

Notation	Definition/explanation
t_c	The playback duration time (seconds) for one chunk
$b_l(q_l)$	The bitrate of viewport tiles in one transcoded chunk with quality $q_l \in Q^{trs}$ for local viewport rendering
$b_l(q_o)$	The bitrate of one original (before transcoding) full-resolution video chunk with quality q_o for local viewport rendering
$b(\Delta q_l)$	The bitrate of the standby tiles in one transcoded chunk with quality $\Delta q_l \in Q^{trs}$ for local viewport rendering
$b_f(q_o)$	The bitrate of one original (before transcoding) full-resolution video chunk with quality q_o for mobile edge viewport rendering
$b(\Delta q_f)$	The bitrate of the standby tiles for one transcoded chunk with quality $\Delta q_f \in Q^{trs}$ for mobile edge viewport rendering
$b_f^r(q_f)$	The bitrate of viewport data in one transcoded chunk with quality $q_f \in Q^{trs}$ for mobile edge viewport rendering
$x_v^o(q_o)$	The viewport tile data volume in t_c after decoding the original data
$x_s^o(q_o)$	The standby tile data volume in t_c after decoding the original data
$x_r^o(q_o)$	The data volume of the rendered viewport in t_c after decoding the original data
v_l^{de}	The PVRV decoding speed on the mobile device
v_f^{de}	The PVRV decoding speed on the MEC server
v_f^{en}	The PVRV encoding speed on the MEC server
b_{zf}	The computed data volume in one CPU cycle on the MEC server
b_{zl}	The computed data volume (given in bits) in one CPU cycle on the mobile device
z_l	The computation capability (cycles/second) of mobile device CPU
z_f	The computation capability (cycles/second) of MEC server CPU

be carefully analyzed. For simplifying notation, we use the term q_l to denote the quality representation $q_l(\pi_l)$. The notation for the other quality representations are also similarly simplified in the remaining of this paper. For ease of reference, all the notations introduced in this subsection are listed in Table I.

1) Local Viewport Rendering for the Sub-6 GHz Band: In this case, the delivered data representation corresponds to case (A) in Fig. 3. For a session that starts from the request of the viewport until its rendering, there are typically several necessary data-processing steps: first transcoding the original chunk on the MEC server, then transmitting the transcoded chunk from the MEC server to the UE, decoding the received chunk and also rendering the viewport on the mobile device. Recall our assumption that all the requested PVRV tiles have already previously been cached at the MEC server which means that the data delivery latency from source provider to the MEC server should not be included in the overall latency.

Assume that the computation task $d_l(b_l(q_l)\cdot t_c)$ for rendering the viewport for a chunk on the mobile device requires $\frac{b_l(q_l)\cdot t_c}{b_{zl}}$ CPU cycles. To finish this task, the UE needs to request the full-resolution chunk data of $[b_l(q_l)+b(\Delta q_l)]\cdot t_c$ bits from the MEC server, where $b_l(q_l)\cdot t_c$ and $b(\Delta q_l)\cdot t_c$ are the numbers of bits of viewport and standby tiles, respectively. Transmitting the requested chunk over the sub-6 GHz link from the MEC server to UE requires $\frac{[b_l(q_l)+b(\Delta q_l)]\cdot t_c}{G_{sub\text{-}6GHz}(m)}$ seconds. For preparing the requested data of a chunk, transcoding on the MEC server will be dedicated to two tasks: the original PVRV data decoding that requires time $\frac{b_l(q_o)\cdot t_c}{v_f^{de}}$ and the PVRV data re-encoding that consumes time equal to $\frac{[b_l(q_l)+b(\Delta q_l)]\cdot t_c}{v_f^{en}}$. On the mobile device, decoding the received viewport data requires $\frac{b_l(q_l)\cdot t_c}{v_l^{de}}$ seconds and the viewport rendering is then finished in $\frac{b_l(q_l)\cdot t_c}{z_l\cdot b_{zl}}$ seconds. The standby tile data will be decoded on the mobile device only when it is used for rendering a new viewport. Consequently, the decoding time for standby tiles does not have to be included in the latency computation for a viewport requesting session. Thus, the overall latency from time the chunk is requested to the display of the viewport is written as

$$t_l = \frac{[b_l(q_l)+b(\Delta q_l)]\cdot t_c}{G_{sub\text{-}6GHz}(m)} + \frac{b_l(q_o)\cdot t_c}{v_f^{de}} + \frac{[b_l(q_l)+b(\Delta q_l)]\cdot t_c}{v_f^{en}} + \frac{b_l(q_l)\cdot t_c}{v_l^{de}} + \frac{b_l(q_l)\cdot t_c}{z_l\cdot b_{zl}} \quad (9)$$

Regarding energy, the first component of the required energy is spent on data reception. The energy for receiving data volume $[b_l(q_l)+b(\Delta q_l)]\cdot t_c$ in the UE is computed as [34]

$$e_{rev}([b_l(q_l)+b(\Delta q_l)]\cdot t_c) = \frac{[b_l(q_l)+b(\Delta q_l)]\cdot t_c \cdot P_b}{b_{rev}}, \quad (10)$$

where P_b denotes the basic circuit power in one second and b_{rev} is the receiving data rate for the UE. Similarly, the PVRV viewport tile data decoding on the mobile device will also consume energy and that is computed as [35]

$$e_{de}(b_l(q_l)\cdot t_c) = \mu^2 E_0, \quad (11)$$

where μ is the frequency scaling factor that is related to the number of decoder data bits $b_l(q_l)\cdot t_c$, and E_0 is the energy that is consumed for a task without any frequency scaling.

Besides the above task, the viewport rendering will also consume energy and it is calculated as $\xi\cdot\frac{b_l(q_l)\cdot t_c}{z_l\cdot b_{zl}}$, where ξ (joules/second) denotes the consumed energy in one second within the CPU computation capability z_l. Therefore, the total energy that is consumed for local viewport rendering on a mobile device is calculated as

$$e_l = e_{rev}([b_l(q_l)+b(\Delta q_l)]\cdot t_c) + e_{de}(b_l(q_l)\cdot t_c) + \xi\cdot\frac{b_l(q_l)\cdot t_c}{z_l\cdot b_{zl}} \quad (12)$$

2) Mobile Edge Viewport Rendering for the Sub-6 GHz Band: When the viewport rendering is finished on the MEC server, decoding the original chunk data and re-encoding the viewport data and the standby tiles are also needed. This specific transcoding route corresponds to part (B) in Fig. 3.

Now let us assume the original data representation of PVRV with bitrate $b_f(q_o)$ is used for transcoding. The PVRV decoding on the MEC server requires $\frac{b_f(q_o)\cdot t_c}{v_f^{de}}$ seconds. Next, task $d_f(b_f^r(q_f)\cdot t_c)$ that is responsible for rendering the viewport on the MEC server needs $\frac{b_f^r(q_f)\cdot t_c}{b_{zf}}$ CPU cycles and it will take $\frac{b_f^r(q_f)\cdot t_c}{z_f\cdot b_{zf}}$ seconds. Furthermore, depending on the processing

power of the MEC server, encoding the rendered viewport and also the standby tiles will take $\frac{[b_f^r(q_f)+b(\Delta q_f)]\cdot t_c}{v_f^{en}}$ seconds. Finally, decoding the viewport data on the mobile device will require $\frac{b_f^r(q_f)\cdot t_c}{v_l^{de}}$ seconds. Thus, adding the transmission time the total time for requesting a viewport with mobile edge viewport rendering is

$$t_f = \frac{b_f(q_o)\cdot t_c}{v_f^{de}} + \frac{b_f^r(q_f)\cdot t_c}{z_f \cdot b_{zf}} + \frac{[b_f^r(q_f)+b(\Delta q_f)]\cdot t_c}{v_f^{en}} + \frac{b_f^r(q_f)\cdot t_c}{v_l^{de}} + \frac{[b_f^r(q_f)+b(\Delta q_f)]\cdot t_c}{G_{sub\text{-}6GHz}(m)} \quad (13)$$

Now at the mobile device, for the case of a sub-6 GHz link only two computational tasks are needed in a session with mobile edge viewport rendering. The first corresponds to the reception of $[b_f^r(q_f)+b(\Delta q_f)]\cdot t_c$ bits which is negligible in time and consumes energy of $e_{rev}([b_f^r(q_f)+b(\Delta q_f)]\cdot t_c)$ joules (it is computed similar to (10)). The other task corresponds to the decoding of the viewport data bits $b_f^r(q_f)\cdot t_c$ and the resulting energy consumption $e_{de}(b_f^r(q_f)\cdot t_c)$ can be computed similar to (11). Hence, the energy that is consumed on the mobile device is

$$e_f = e_{rev}([b_f^r(q_f)+b(\Delta q_f)]\cdot t_c) + e_{de}(b_f^r(q_f)\cdot t_c) \quad (14)$$

3) Local Viewport Rendering for the mmWave Band: Recall that the goodput estimate of the mmWave link is $G_{mmW}(m)$. Unlike the case of sub-6 GHz link, uncompressed viewport video data are transmitted over the mmWave link. The data preparation follows path (D) in Fig. 3. The needed tasks in a viewport requesting session include decoding the original data representation on the MEC server, transmitting the uncompressed PVRV data over the mmWave band, and rendering the viewport on the mobile device.

Before the data transmission, decoding $b_f(q_o)\cdot t_c$ bits to obtain the uncompressed $x_v^o(q_o)+x_s^o(q_o)$ bits on the MEC server requires $\frac{b_f(q_o)\cdot t_c}{v_f^{de}}$ seconds. At the mobile device, the local viewport rendering will consume $\frac{x_v^o(q_o)}{z_l\cdot b_{zl}}$ seconds. So the overall latency is

$$t_l = \frac{x_v^o(q_o)+x_s^o(q_o)}{G_{mmW}(m)} + \frac{b_f(q_o)\cdot t_c}{v_f^{de}} + \frac{x_v^o(q_o)}{z_l\cdot b_{zl}} \quad (15)$$

In the case of local viewport rendering the energy model for the mmWave band is similar to that for sub-6 GHz band. Since uncompressed data are delivered over the mmWave band, no decoding is necessary on the mobile device. The energy is then equal to

$$e_l = e_{rev}(x_v^o(q_o)+x_s^o(q_o)) + \xi\cdot\frac{x_v^o(q_o)}{z_l\cdot b_{zl}} \quad (16)$$

4) Mobile Edge Viewport Rendering for mmWave Band: According to (C) in Fig. 3, with the mobile edge viewport rendering for the mmWave band, the necessary computation tasks on the MEC server include decoding the original data and rendering the viewport. The only one task on the mobile device is to receive the PVRV data when the viewport that is rendered on the MEC server perfectly matches the one the user requests. Usually, this task is completed in a very short and negligible time. Together with the time for data communication, the overall latency for requesting a viewport is

$$t_f = \frac{b_f(q_o)\cdot t_c}{v_f^{de}} + \frac{x_r^o(q_o)+x_s^o(q_o)}{G_{mmW}(m)} + \frac{x_v^o(q_o)}{z_f\cdot b_{zf}} \quad (17)$$

Since only the task for receiving data is necessary on the mobile device, the required energy is

$$e_f = e_{rev}(x_r^o(q_o)+x_s^o(q_o)) \quad (18)$$

A note regarding user requests: It is important to stress that in this work, we estimate in advance the PVRV system latency and the UE energy consumption under different system parameter configurations. The computations are based on the assumption that the already delivered viewport match the one the user requests. In practical PVRV streaming, the already delivered viewport does not always match that the user requests. In such cases, the low quality standby tiles are used for rendering the necessary viewport on the mobile device. Since these cases are very hard to predict we do not consider them at the cost of missing minor potential performance improvements.

IV. Problem Optimization and Solution

With the proposed system model we desire to find a trade-off between the quality of the received PVRV viewport and the energy cost at the UE. To simplify this problem, the best way is to break the system optimization into two stages. The first stage consists of choosing the appropriate link for PVRV transmission. Then link scheduling is executed as described in the subsection C of Section III. In the second stage, link adaptation is jointly optimized with the adaptive offloading of the viewport rendering.

In the proposed scheme, the decision to offload the viewport rendering or not depends on the trade-off between the energy consumption and the corresponding transmission latency. During PVRV streaming, the viewport is dynamically moved so that the system latency is constrained to one threshold value denoted by $T_{\max}$. Current literature review [13] suggests that the viewport response latency should be less than 10ms when the HMD refresh rate is up to 120 Hz. In such a case, it requires PVRV to be captured with 120 frames per second (fps). However, current PVRV applications in mobile devices use 30 fps as the input data rate of the HMD to seek an early-stage immersive experience [4]. For these cases, $T_{\max}$ is approximately 35 ms. Also in this case since low-quality tiles outside the viewport are always delivered to the UE, the UE can play the viewport video smoothly.

At the physical layer the MCS is adaptively tuned to cater for the chunk quality selection in the sub-6 GHz band or the unequal tile protection in the mmWave band. Hence, two optimization objectives need to be satisfied at the same time. The first is to maximize the quality of the chunk that is delivered, and the second to minimize the energy cost of the mobile de-

vice for rendering the chunk. For the first objective, since chunk quality is a discrete value that is usually greater than zero, maximizing q can be transformed to a minimization of $\frac{1}{q}$. By using multiple-objective combinational optimization theory [36], the above optimization problem can be formulated as a two objective problem: $O1$ for minimizing the energy consumption and $O2$ for maximizing the quality of the received viewport,

$$\begin{aligned} O1: & \min_{\{m,q,\eta\}} \{\eta \cdot e_l + (1-\eta) \cdot e_f\} \\ & \text{s.t. } \eta \cdot t_l + (1-\eta) \cdot t_f < T_{\max} \\ & m = \eta \cdot m_l + (1-\eta) \cdot m_f \\ & q = \eta \cdot q_l + (1-\eta) \cdot q_f \\ & m_l \in M, m_f \in M, q_l \in Q, q_f \in Q, \ \eta \in \{0,1\} \\ O2: & \min \frac{1}{q} \\ & \text{s.t. } \eta \cdot t_l + (1-\eta) \cdot t_f < T_{\max} \\ & q = \eta \cdot q_l + (1-\eta) \cdot q_f \\ & q_l \in Q, q_f \in Q, \ \eta \in \{0,1\} \end{aligned} \tag{19}$$

In the above the notation $M = M_s$ corresponds to sub-6 GHz communication and $M = M_{mm}$ to mmWave communication. M_s and M_{mm} are the candidate MCS sets for sub-6 GHz and mmWave bands, respectively. m_l and m_f are the MCS modes for cases of local and mobile edge viewport rendering, respectively. In this optimization, we assume that the MCS does not change during the transmission of one chunk and thus the MCS selection is synchronized with chunk selection.

In (19), q_l and q_f are the chunk qualities of the viewport tiles that are selected for local and mobile edge viewport rendering, respectively. To reduce the variables in the solution vector, we assume that the chunk quality of the non-viewport tiles is $\Delta q_l = \vartheta_l \cdot q_l$ with $\Delta q_l \in Q$ for local viewport rendering, and $\Delta q_f = \vartheta_f \cdot q_f$ with $\Delta q_f \in Q$ for mobile edge viewport rendering. ϑ_l and ϑ_f are the scaling factors between viewport quality and non-viewport quality for local and mobile edge viewport rendering, respectively. Similarly, $Q = \{q_o\}$ for mmWave band and $Q = Q^{trs}$ for sub-6 GHz band. η is a binary variable that indicates viewport rendering offloading or not. When zero, the viewport rendering is offloaded to the MEC server, otherwise the viewport is rendered locally at the mobile device.

The formulation (19) allows to optimally select for each chunk the quality q, the link MCS m, and whether viewport rendering will be offloaded or not with η. In this formulation we notice the multiple objectives and the discrete combinational decisions. Hence, (19) is a constrained multiple objective problem and is NP-hard. For this class of problems, near-optimal solutions (Pareto-optimal solutions [36]) can be found within a bounded amount of time. Genetic algorithms (GA) are a popular meta-heuristic that is particularly well-suited for this type of problems. Due to the computationally fast and elitism strategy in GAs, the non-dominated sorting GA (NSGA II) [37] promises better performance than other GAs. Hence, we use NSGA II to solve the problem in (19). In (19), the vector of variables (m, q, η) is considered as an individual that symbolizes a candidate solution, and the constraints can be used to determine whether the candidate solution is feasible.

Algorithm 1: GA for PVRV Transmission Optimization

Require: $\mathbb{N}_{gen}, O1(\mathcal{X}), O2(\mathcal{X}), \mathcal{X} = (m, q, \eta)$
Ensure: The optimal solution $\mathcal{X}_{opt}$
1: Generate the initial parent population U_0;
2: Evaluate the objective functions for each individuals in U_0 to obtain $O1(\mathcal{X}_i)$ and $O2(\mathcal{X}_i)$ from $i = 1$ to $\mathbb{N}$;
3: Perform the binary tournament, crossover and mutation operators to create the offspring population V_0 of size $\mathbb{N}$;
4: **for** $i < \mathbb{N}_{gen}$ **do**
5: Fast non-dominated-sorting for the combined population of the parent and offspring $R_i = U_i \cup V_i$ of size $2\mathbb{N}$;
6: Crowding distance sorting;
7: Perform selection operation to obtain U_{i+1} of size $\mathbb{N}$ by crowded-comparison operator;
8: Perform crossover and mutation operation to generate V_{i+1} of size $\mathbb{N}$;
9: $i = i + 1$;
10: **end for**

The proposed optimization scheme is performed in real-time for each chunk and the optimization is executed once during the chunk playback. The GA for the transmission optimization of each chunk is shown in Algorithm 1. Initially, the number of population generations $\mathbb{N}_{gen}$ and the objective functions are initialized. In the following steps, the initial parent population that includes $\mathbb{N}$ individuals (namely $\mathcal{X}_1, \mathcal{X}_2, ...\mathcal{X}_i, \ldots, \mathcal{X}_{\mathbb{N}}$) is generated. After computing the fitness (objective function) values for all the individuals in the initial population, the binary tournament, crossover, and mutation are executed sequentially on the initial population to create the offspring population. In the next step, the combinational ith-generation population $R_i = U_i \cup V_i$ of size $2\mathbb{N}$ is obtained. The operations of non-dominated sorting and crowding-distance sorting are executed on the set R_i. The next generation populations U_{i+1} and V_{i+1} are then obtained by the crowded-comparison operator, crossover and mutation, respectively. The procedure for generating V_{i+1} will be recursively executed until $i = \mathbb{N}_{gen}$. Finally, the optimal solution will be selected from the population of the last generation.

V. Simulation and Evaluation

Ns-3 was used to simulate the MC-based mmWave communication scheme [8]. The different layers of the LTE and mmWave protocol stacks were extended from their respective counterparts of the ns-3 LTE module and mmWave stacks [33] and they were modified to create the dual-radio framework [44]. A UDP-like streaming service for the PVRV packets over the MC-based mmWave framework was also implemented. According to the user's head motion recordings for requesting the PVRV tiles, the data packets of tiled chunks were delivered over the MC-based mmWave framework. During the simulation, the streaming trace

TABLE II
SIMULATION PARAMETERS

Q^{trs}	{2Mbps, 6Mbps, 10Mbps, 15Mbps, 20Mbps, 25Mbps, 30Mbps, 36Mbps}
M_s	Follow those in [30]
M_{mm}	Follow those in [33][44]
b_{zf}	500Mb
b_{zl}	5Mb
z_f	1000GHz
z_l	0.5GHz
t_c	0.133s
v_f^{en}	3Gbps
v_f^{de}	30Gbps
v_l^{de}	300Mbps
ξ	0.8 Joules/second
P_b	10Watt [34]
μ	0.5
E_0	1.06Watt [35]
b_{re}	300Mbps

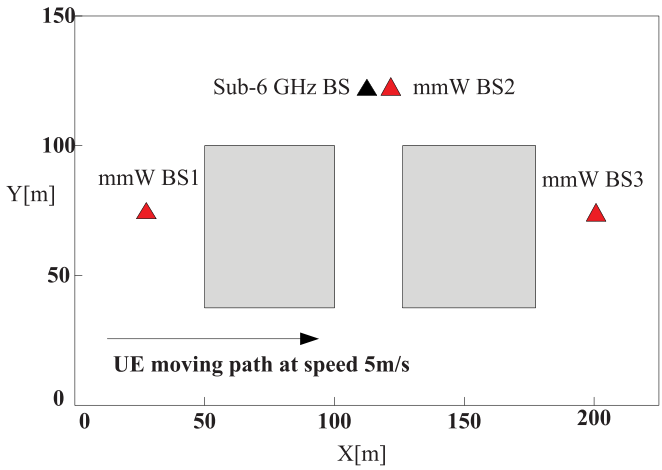

Fig. 6. One example of the simulated urban environments. The grey rectangles indicate buildings.

data were recorded. The simulation trace data were finally used to reconstruct the PVRV playback for evaluating the viewport quality, the latency and the energy performances.

We also implemented the real-time PVRV transcoding module by using the high efficiency video coding (HEVC) model. The MEC server in Fig. 2 was modeled by assuming one cache server in which the viewport rendering and transcoding modules were implemented. Table II shows the detailed simulation parameters that were used for the proposed PVRV streaming system. The link qualities in terms of SINR values were collected under different urban environments where the buildings were randomly deployed affecting thus considerably channel dynamics in the mmWave band [8]. One example of the simulated deployments of the city buildings is shown in Fig. 6. There are two buildings and each of them is 15 meters high. Three mmWave BSs are located at coordinates BS1 = (25, 75), BS2 = (110, 125) and BS3 = (200, 75), at a height of 10 meters. The sub-6 GHz BS is co-located with mmWave BS2. In the simulation, one UE moved from (0, 25) to (200, 25) along the x-axis with a speed of 5 meter per second.

TABLE III
VIEWPORT TRAJECTORIES IN THE SIMULATION

Trajectory number	Start position (longitude, altitude)	End position (longitude, altitude)
1	(90, -180)	(-89,180)
2	(75,75)	(-75,-150)
3	(60, -30)	(-60,-120)
4	(-30,180)	(75,-45)
5	(-75,75)	(-80, 120)
6	(45,-135)	(-135,75)
7	(-5,20)	(-90, -175)
8	(-20,-90)	(45,165)

Regarding the content, several PVRV datasets [38]–[41] are available with realistic head movement traces for exploring user viewing behavior patterns in PVRV applications. Unfortunately, these PVRV datasets provided the compressed formats, but not the original YUV data. Consequently, the computation of the peak signal to noise ratio of the viewport (VPSNR) for these PVRVs is infeasible since they lack the original signal needed for reference. Consequently, we used 4K PVRV clips with 300 frames from MPEG [42]. In particular, the used video clips include DrivingInCity, AerialCity, DrivingInCountry and PoleVault_le. The viewport was extracted by the 360lib software provide by MPEG [43]. Different viewport trajectories with random and dynamic viewport modes were used for evaluating streaming performance. The statistics on the users' viewport movements [39] show that users typically change their viewport once significantly (The viewport tiles are changed) with an interval that is ranged from 2 frames to more than 30 frames. Consequently, given a start-up position of viewport at the first frame and an end position of viewport at the last frame, viewport trajectories with different switching frequencies from 1 Hz to 15 Hz were recorded for simulating PVRV streaming. The start and end positions of viewport are listed in Table III. The viewport size was set to 856 × 856. A total of three simulations were executed for each viewport trajectory and the average result over three runs is presented. Since only one viewport is watched by the end-user at a specific moment, the VPSNR between the viewport that is rendered from the original PVRV and the one that is rendered from the received PVRV is computed to evaluate streaming performance.

We compared the performance of the proposed MEC-assisted mmWave PVRV streaming scheme (mc-mmW-w-MEC) with several reference scenarios. The first one considers sub-6 GHz PVRV streaming with MEC (sub-6GHz-w-MEC). The second adopts MC-based mmWave streaming without MEC (mc-mmW-w/o-MEC).

A. PVRV Streaming Performance

1) Mobile Edge Transcoding: Fig. 7 (a) and (b) show the viewport qualities in terms of VPSNR for unequal quality transcoding of mc-mmW-w-MEC, equal quality transcoding of mc-mmW-w-MEC, and mc-mmW-w/o-MEC (no transcoding) schemes for an average channel SINR of 20 dB and 30 dB, respectively. For each video clip the average VPSNR value over all viewport paths was measured. It can be seen in Fig. 7 that

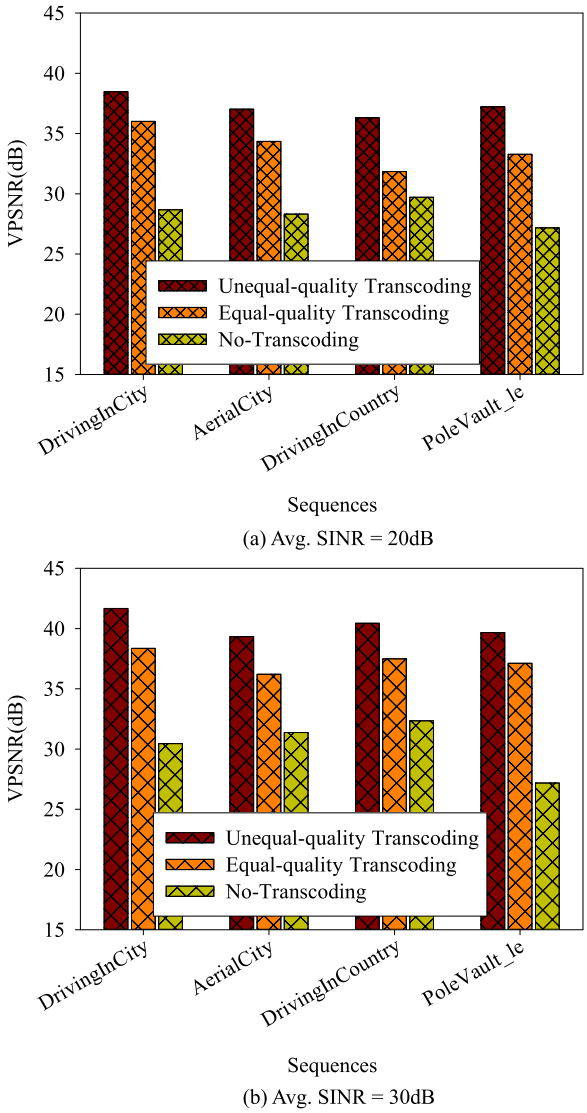

Fig. 7. Viewport quality comparisons for different streaming schemes.

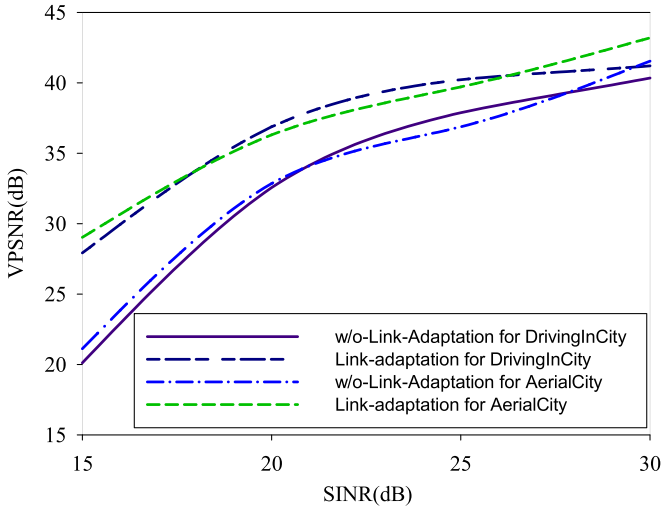

Fig. 8. The link adaptation efficiencies under different networking conditions.

the proposed unequal quality transcoding offers superior quality over equal quality transcoding and the streaming scheme without transcoding. The quality improvements of the proposed scheme over mc-mmW-w/o-MEC, indicate that the MEC plays a crucial role in quality optimization (MEC enabled real-time transcoding or processing for PVRV quality optimization) of PVRV streaming. At the same time, the results also demonstrate that unequal quality allocation over the tiles in the image, can improve the viewport quality subject to the limited available bandwidth.

2) Link Adaptation: In the proposed scheme, viewport-optimized link adaptation is used to ensure the tight coupling between the streaming PVRV bitrate and the available link bandwidth. Fig. 8 shows the impact of link adaptation under different network conditions (in terms of the average SINR value). This figure clearly illustrates that link adaptation is very efficient (at least 30% better) particularly at low SINR (15 dB), while in the high SINR regime (around 30 dB) performance benefits are also significant (at least 3 dB).

3) Quality of the Received Viewport: To evaluate the overall performance of the proposed scheme, we measured the quality of the received viewport for our scheme and the reference schemes. The average VPSNR values for different viewport trajectories are plotted in Fig. 9. The results indicate the clear benefits of the proposed scheme over all the other schemes. The reason is that the proposed mc-mmW-w-MEC system exploits to the fullest not only the high capacity of the mmWave link with conquering the interruptions but also the computational capabilities of the MEC server.

B. Latency

System latency is a key performance indicator of the PVRV system. During our simulations we recorded the latency of each viewport request. Fig. 10 shows the instantaneous latency results for one viewport trajectory for streaming DrivingInCity clip. The proposed scheme has a clear advantage over the other schemes in terms of system latency. After collecting extensive data sets of the viewport latency we plot in Fig. 11 the cumulative distribution functions (CDF) of this viewport request latency for different viewport trajectories and over all PVRV clips. As illustrated in Fig. 11, during 60% of the time, the proposed scheme achieves a viewport request latency less than 20 ms. The competing schemes achieve the viewport request latency of less than 20ms for only 20% of the time. Also, it is interesting to note that the schemes with MEC achieve lower latency than those without MEC, something that it is indicative of its contribution to the overall latency.

C. UE Energy Consumption

We also conducted extensive UE energy measurements under different viewport switching frequencies. For each viewport switching frequency we measured the ratio between computa-

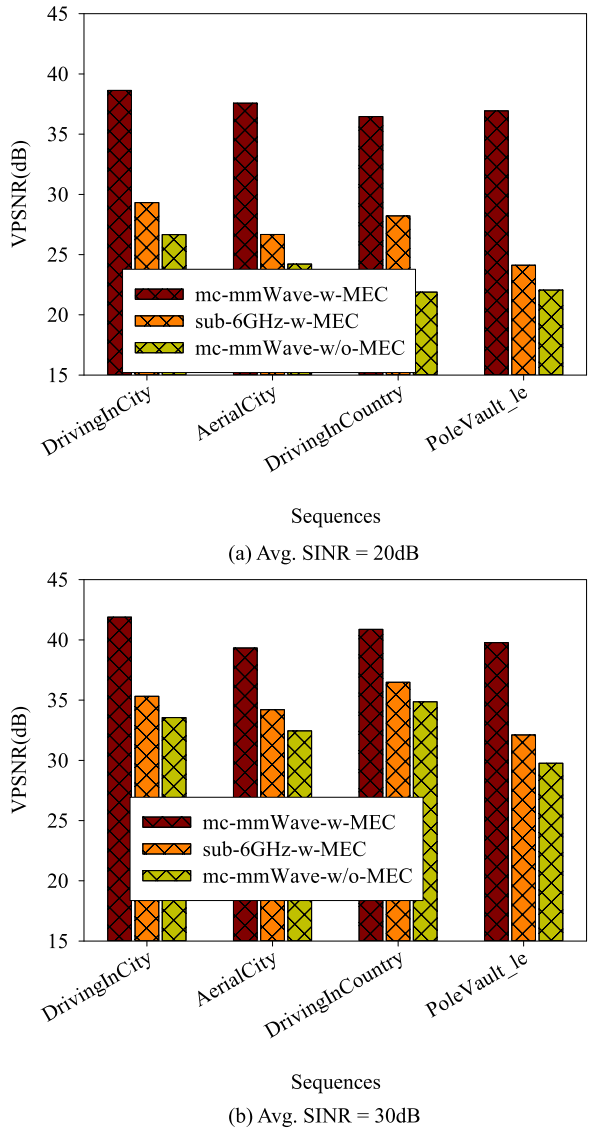

Fig. 9. The quality of the received viewport. (a) Avg. SINR = 20 dB (b) Avg. SINR = 30 dB

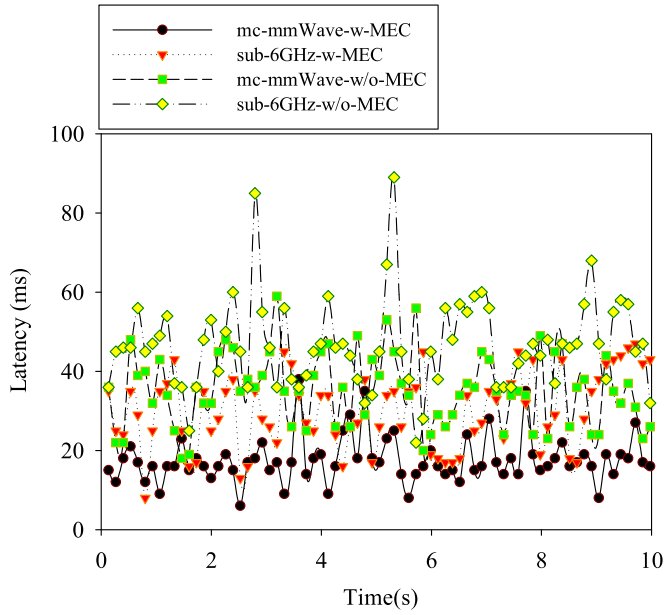

Fig. 10. The viewport latency for one trajectory at SINR of 30 dB.

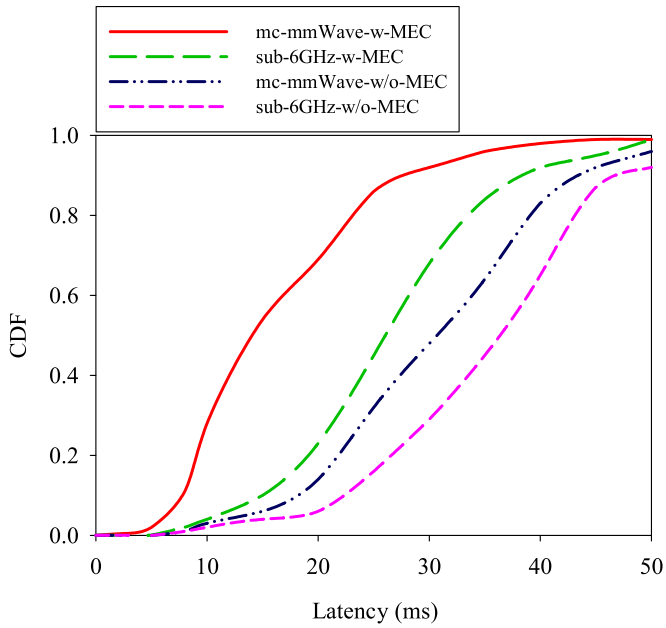

Fig. 11. The CDF of viewport-request latency at SINR of 30 dB.

tions of the viewport rendering on the MEC server and the total computations for viewport rendering that were performed on both the MEC and the UE (for all video clips). We named this ratio "the viewport rendering offloading ratio", as shown in the left side of Fig. 12(a). The energy-saving ratio between the UE energy of the proposed mc-mmWave-w-MEC and that of mc-mmWave-w-MEC without viewport rendering offloading is also computed over all different viewport switching frequencies. It is shown in the right side of Fig. 12(a). The average wireless SINR for the results of Fig. 12(a) is 30 dB. The energy-saving ratio is gradually reduced with increasing viewport switching frequency and an average of 30% energy reduction is achieved for viewport rendering over all viewport switching frequencies. This indicates that the ratio of viewport rendering offloading is gradually reduced with more frequent viewport switchings and this exactly matches with the curve in the left side of Fig. 12(a). When the viewport moves faster, the pre-rendered viewport at the MEC server will not match the actual browsing viewport and thus more viewport rendering operations will be executed at the UE. Consequently the energy consumption is increased.

At a viewport switching frequency of 4Hz, we computed the viewport rendering offloading ratio and the energy-saving ratio over all video clips, and the results are shown in Fig. 12(b). Both metrics increase with improving link quality. For high link quality, the goodput is relatively larger than that for low link quality. Hence, the transmission time for the rendered viewport is reduced accordingly and the optimization will be more inclined to offload the viewport rendering to the MEC server. This energy curve follows a similar pattern with the offloading ratio.

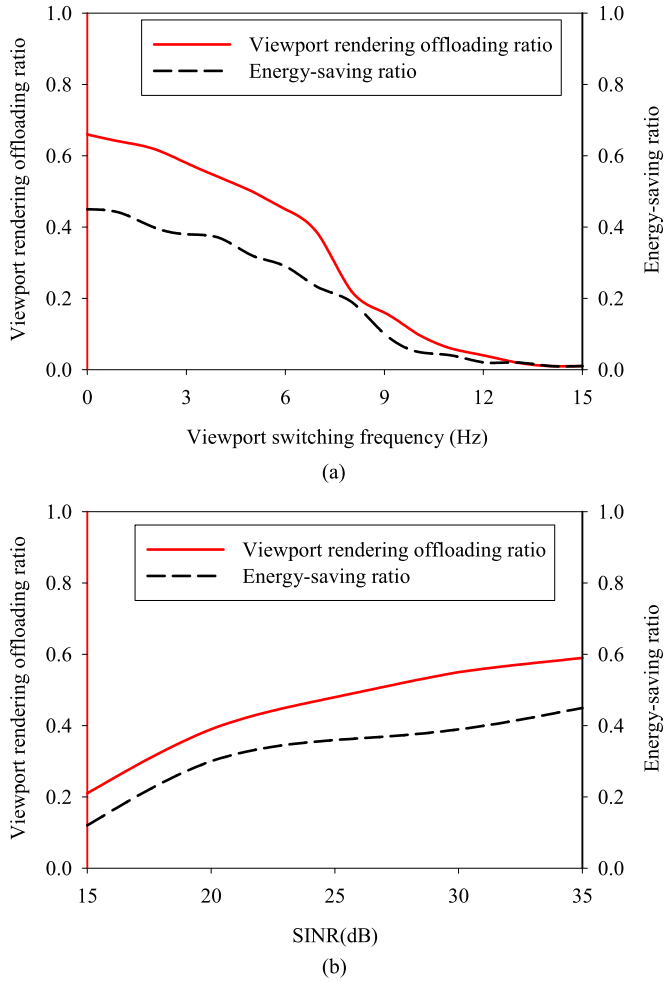

Fig. 12. The energy-saving ratio and viewport rendering offloading ratio (a) for different viewport switching frequency and (b) for different SINR values.

VI. Conclusion

In this paper we presented an MEC-assisted PVRV streaming scheme that is designed to operate over MC-based mmWave mobile networks. By complementing the mmWave link with sub-6 GHz wireless communication, the MC-based mmWave mobile network offers both sufficient bandwidth and steady communication for PVRV streaming. Furthermore, we introduced MEC as an intermediate processing component not only to enable real-time transcoding to offer the appropriate PVRV representations for the matched transmission links, but also to execute real-time viewport rendering computations that reduce the energy consumption of the UE. Through MEC, the delivery of a PVRV representation is tightly coupled with the specific link so as to maximize the utilization of the wireless bandwidth. A comprehensive optimization that jointly optimizes the video chunk quality, link adaptation, and adaptive viewport rendering offloading is casted as a multi-objective optimization problem that is solved by a fast GA. Simulation results demonstrate that the proposed scheme can improve the PVRV streaming performance significantly over the traditional schemes in system latency, energy efficiency, and the quality of the received viewport.

References

[1] MPEG Experts, "Summary of survey on virtual reality," ISO/IEC JTC 1/SC 29/WG 11, m16542, Chengdu, China, Oct. 2016.

[2] Qualcomm Technologies Inc., "Whitepaper: Making immersive virtual reality possible in mobile," Mar. 2016. [Online]. Available: https://www.qualcomm.com/.

[3] Y. Bao, T. Zhang, A. Pande, H. Wu, and X. Liu, "Motion-prediction-based multicast for 360-Degree video transmissions," in *Proc. 4th Annu. IEEE Int. Conf. Sens. Commun. Netw.*, 2017, pp. 1–9.

[4] Huawei-ilab, "Whitepaper on the VR-Oriented Bearer Network Requirement," Sep. 2016. [Online]. Available: http://www.huawei.com/

[5] M. Yu, H. Lakshman, and B. Girod, "A framework to evaluate omnidirectional video coding schemes," in *Proc. IEEE Int. Symp. Mixed Augmented Reality*, 2015, pp. 31–36.

[6] ABI Research Report, "Display Technologies in Virtual Reality," 3Q 2017.

[7] W. Roh *et al.*, "Millimeter-wave beamforming as an enabling technology for 5G cellular communications: Theoretical feasibility and prototype results," *IEEE Commun. Mag.*, vol. 52, no. 2, pp. 106–113, Feb. 2014.

[8] M. Polese, M. Giordani, M. Mezzavilla, S. Rangan, and M. Zorzi, "Improved handover through dual connectivity in 5g mmWave mobile networks," *IEEE J. Sel. Areas Commun.*, vol. 35, no. 9, pp. 2069–2084, Sep. 2017.

[9] M. Patel *et al.*, "Mobile-edge computing-introductory technical white paper," *ETSI white paper*, no. 1, pp. 1–36, Sep. 2014.

[10] M. Budagavi *et al.*, "360 degrees video coding using region adaptive smoothing," in *Proc. IEEE Int. Conf. Image Process.*, 2015, pp. 750–754.

[11] Y. Sánchez, R. Skupin, and T. Schierl, "Compressed domain video processing for tile based panoramic streaming using HEVC," in *Proc. IEEE Int. Conf. Image Process.*, Quebec City, QC, Canada, Sep. 2015, pp. 2244–2248.

[12] M. Yu, H. Lakshman, and B. Girod, "Content adaptive representations of omnidirectional videos for cinematic virtual reality," in *Proc. 3rd Int. Workshop Immersive Media Experiences*, Brisbane, Australia, Nov. 2015, pp. 1–6.

[13] X. Corbillon *et al.*, "Viewport-adaptive navigable 360-degree video delivery," in *Proc. IEEE Int. Conf. Commun.*, 2017, pp. 1–7.

[14] K.-T. Ng, S.-C. Chan, and H.-Y. Shum, "Data compression and transmission aspects of panoramic videos," *IEEE Trans. Circuits Syst. Video Technol.*, vol. 15, no. 1, pp. 82–95, Jan. 2005.

[15] V. R. Gaddam *et al.*, "Tiling in interactive panoramic video approaches and evaluation," *IEEE Trans. Multimedia*, vol. 18, no. 9, pp. 1819–1831, Sep. 2016.

[16] M. Xiao, C. Zhou, Y. Liu, and S. Chen, "OpTile: Toward optimal tiling in 360-degree video streaming," in *Proc. ACM Multimedia Conf.*, Mountain View, CA, USA, Oct. 23–27, 2017, pp. 708–716.

[17] S. Petrangeli, V. Swaminathan, M. Hosseini, and F. Turck, "An HTTP/2-based adaptive streaming framework for 360° virtual reality videos," in *Proc. ACM Multimedia Conf.*, Mountain View, CA, USA, Oct. 2017, pp. 306–314.

[18] L. Xie, Z. Xu, Y. Ban, X. Zhang, and Z. Guo, "360ProbDASH: Improving QoE of 360 video streaming using tile-based HTTP adaptive streaming," in *Proc. ACM Multimedia Conf.*, Mountain View, CA, USA, Oct. 2017, pp. 315–323.

[19] H. Singh *et al.*, "A 60 GHz wireless network for enabling uncompressed video communication," *IEEE Commun. Mag.*, vol. 46, no. 12, pp. 71–78, Dec. 2008.

[20] J. Qiao, X. Shen, J. W. Mark, and L. Lei, "Video quality provisioning for millimeter wave 5g cellular networks with link outage," *IEEE Trans. Wireless Commun.*, vol. 14, no. 10, pp. 5692–5703, Oct. 2015.

[21] M. Choi *et al.*, "Link adaptation for high-quality uncompressed video streaming in 60-GHz wireless networks," *IEEE Trans. Multimedia*, vol. 18, no. 4, pp. 627–642, Apr. 2016.

[22] O. Abari, D. Bharadia, A. Duffield, and D. Katabi, "Enabling high-quality untethered virtual reality," in *Proc. 14th USENIX Symp. Netw. Syst. Des. Implementation*, Boston, MA, USA, Mar. 27–29, 2017, pp. 531–544.

[23] J. Kim, J. Lee, and W. Lee, "Strategic control of 60 GHz millimeter-wave high-speed wireless links for distributed virtual reality platforms," *Mobile Inf. Syst.*, vol. 2017, Art. no. 5040347, 2017.

[24] C. Chang *et al.*, "MEC architectural implications for LTE/LTE-A networks," in *Proc. Workshop Mobility Evolving Internet Archit.*, New York City, NY, USA, Oct. 3–7, 2016, pp. 13–18.

[25] ETSI GS MEC 012, "Mobile edge computing (MEC); radio network information API," Jul. 2017.

[26] E. Bastuğ, M. Bennis, and M. Debbah, "Living on the edge: The role of proactive caching in 5g wireless networks," *IEEE Commun. Mag.*, vol. 52, no. 8, pp. 82–89, Aug. 2014.
[27] C. Herglotz, A. Heindel, and A. Kaup, "Decoding-energy-rate-distortion optimization for video coding," *IEEE Trans. Circuits Syst. Video Technol.*, 2017, doi: 10.1109/TCSVT.2017.2771819.
[28] 3GPP, "Technical specification group radio access network; Study on small cell enhancement for (E-UTRA) and (e-TRAN); Higher layer aspects (Release 12), TR 36.842, 2013.
[29] Z. Shen, J. G. Andrews, and B. L. Evans, "Adaptive resource allocation in multiuser OFDM systems with proportional rate constraints," *IEEE Trans. Wireless Commun.*, vol. 4, no. 6, pp. 2726–2737, Nov. 2005.
[30] P. Zhao *et al.*, "SSIM-based cross-layer optimized video streaming over LTE downlink," in *Proc. IEEE Global Commun. Conf.*, Auxtin, TX, USA, Dec. 8–12, 2014, pp. 1394–1399.
[31] M. Woltering, D. Wbben, A. Dekorsy, V. Braun, and U. Doetsch, "Performance of HARQ with reduced size retransmissions using network coding principles," in *Proc. IEEE 77th Veh. Technol. Conf.*, 2013, pp. 1–6.
[32] K. Liu, Y. Liu, J. Liu, A. Argyriou, and X. Yang, "Joint source encoding and networking optimization for panoramic video streaming over LTE-A downlink," in *Proc. IEEE Global Commun. Conf.*, Singapore, Dec. 4–8, 2017, pp. 1–7.
[33] M. Mezzavilla, S. Dutta, M. Zhang, M. Akdeniz, and S. Rangan, "5G MmWave module for the ns-3 network simulator," in *Proc. 18th ACM Int. Conf. Model. Anal. Simul. Wireless Mobile Syst.*, Cancun, Mexico, pp. 283–290.
[34] L. Lei *et al.*, "Resource scheduling to jointly minimize receiving and transmitting energy in OFDMA systems," in *Proc. 11th Int. Symp. Wireless Commun. Syst.*, 2014, pp. 187–191.
[35] Z. Lu *et al.*, "Reducing multimedia decode power using feedback control," in *Proc. Int. Conf. Comput. Des.*, San Jose, CA, USA, Oct. 2003, pp. 489–406.
[36] M. Ehrgott and X. Gandibleux, "Multiple objective combinatorial optimization—A tutorial," in *Multi-Objective Programming and Goal Programming, Advances in Soft Computing*, vol. 21. New York, NY, USA: Springer, 2003.
[37] K. Deb, A. Pratap, S. Agarwal, and T. Meyarivan, "A fast and elitist multiobjective genetic algorithm: NSGA-II," *IEEE Trans. Evol. Comput.*, vol. 6, no. 2, pp. 181–197, Apr. 2002.
[38] C. Wu, Z. Tan, Z. Wang, and S. Yang, "A dataset for exploring user behaviors in VR spherical video streaming," in *Proc. 8th ACM Multimedia Syst. Conf.*, Taipei, Taiwan, Jun. 20–23, 2017, pp. 193–198.
[39] W. Lo *et al.*, "360 video viewing dataset in head-mounted virtual reality," in *Proc. 8th ACM Multimedia Syst. Conf.*, Taipei, Taiwan, Jun. 20–23, 2017, pp. 211–216.
[40] X. Corbillon, F. De Simone, and G. Simon, "360-degree video head movement dataset," in *Proc. 8th ACM Multimedia Syst. Conf.*, Taipei, Taiwan, Jun. 20–23, 2017, pp. 199–204.
[41] Y. Song *et al.*, "Modeling attention in panoramic video: A deep reinforcement learning approach," 2017, arXiv:1710.10755.
[42] E. Alshina, J. Boyce, A. Abbas, and Y. Ye, "JVET common test conditions and evaluation procedures for 360° video," JVET-H1030, Macao, China, Oct. 18–24, 2017.
[43] Y. He, B. Vishwanath, X. Xiu, and Y. Ye, "AHG8: InterDigital's projection format conversion tool," Joint Video Exploration Team of ITU-T SG16 WP3 and ISO/IEC JTC1/SC29/WG11, JVET-D0021, Oct. 2016, Chengdu, China.
[44] M. Mezzavilla *et al.*, "End-to-end simulation of 5G mmWave networks," *IEEE Commun. Surv. Tut.*, vol. 20, no. 3, pp. 2237–2263, Third Quarter 2018.
[45] M. Drago, T. Azzino, M. Polese, C. Stefanovic, and M. Zorzi, "Reliable video streaming over mmWave with multi connectivity and network coding," in *Proc. Int. Conf. Comput. Netw. Commun.*, 2018, pp. 508–512.
[46] S. Amir Hoseini, M. Ding, and M. Hassan, "A new look at MIMO capacity in the millimeter wave," in *Proc. IEEE Global Telecommun. Conf.*, Singapore, Dec. 4–8, 2017, pp. 1–7.

Yanwei Liu (M'14) received the B.S. degree in applied geophysics from Jianghan Petroleum University, Jingzhou, China, in 1998, the M.S. degree in computer science from China Petroleum University, Beijing, China, in 2004 and the Ph.D. degree in computer science from Institute of Computing Technology, Chinese Academy of Sciences, Beijing, China, in 2010. He is currently an Associate Professor with the Institute of Information Engineering, Chinese Academy of Sciences. He has published more than 60 scientific papers. His research interests include digital image/video processing, multiview/3-D video/VR video processing, wireless multimedia networking. Dr. Liu serves on the TPCs of several international conferences in the area of multimedia, communications, and networking.

Jinxia Liu received the B.S. degree and M.S. degree in physics from Harbin Normal University, Harbin, China, in 1994 and 2005, respectively. In 2005, she joined the Zhejiang Wanli University. She is currently a Professor with Zhejiang Wanli University, Ningbo, China. Her research interests include laser imaging, digital image/video processing, multiview and 3-D video coding, and wireless communication.

Antonios Argyriou (S'00–M'07–SM'15) received the Diploma degree in electrical and computer engineering from Democritus University of Thrace, Xanthi, Greece, and the M.S. and Ph.D. degrees in electrical and computer engineering (as a Fulbright Scholar) from Georgia Institute of Technology, Atlanta, GA, USA, in 2001, 2003, and 2005, respectively. He is currently an Assistant Professor with the Department of Electrical and Computer Engineering, University of Thessaly, Volos, Greece. From 2007 to 2010, he was a Senior Research Scientist with Philips Research, Eindhoven, The Netherlands. From 2004 to 2005, he was a Senior Engineer with Soft.Networks, Atlanta, GA, USA. He currently serves on the Editorial Board of the *Journal of Communications*. He has also served as Guest Editor for the IEEE TRANSACTIONS ON MULTIMEDIA Special Issue on Quality-Driven Cross-Layer Design, and he was also a Lead Guest Editor for the *Journal of Communications*, Special Issue on Network Coding and Applications. His research interests include wireless communication systems and networks, and video delivery. Dr. Argyriou serves on the TPCs of several international conferences and workshops in the area of communications, networking, and statistical signal processing.

Song Ci (S'98–M'02–SM'06) received the B.S. degree from the Shandong University of Technology (now Shandong University), Jinan, China, in 1992, the M.S. degree from the Chinese Academy of Sciences, Beijing, China, in 1998, and the Ph.D. degree from the University of Nebraska-Lincoln, Lincoln, NE, USA, in 2002, all in electrical engineering. He is currently an Associate Professor with the Department of Electrical and Computer Engineering, University of Nebraska-Lincoln. He serves as an Editor, Guest Editor or Associate Editor in editorial boards of many journals, including the IEEE TRANSACTIONS ON CIRCUITS AND SYSTEMS FOR VIDEO TECHNOLOGY, the IEEE TRANSACTIONS ON MULTIMEDIA, the IEEE TRANSACTIONS ON VEHICULAR TECHNOLOGY, and the IEEE ACCESS. His current research interests include dynamic complex system modeling and optimization, content-aware quality-driven cross-layer optimized multimedia over wireless, energy internet, and green computing. Prof. Ci also serves as the TPC member for numerous conferences. He is a member of ACM and AAAS.